The Astrophysical Journal Letters, 719:L56–L59, 2010 August 10 doi:10.1088/2041-8205/719/1/L56

NONLINEAR FORCE-FREE MODELING OF MAGNETIC FIELDS IN A SOLAR FILAMENT

Ju Jing[1], Yuan Yuan[1], Thomas Wiegelmann[2], Yan Xu[1], Rui Liu[1], and Haimin Wang[1]
[1] Space Weather Research Laboratory, New Jersey Institute of Technology, Newark, NJ 07102, USA; ju.jing@njit.edu, yy46@njit.edu, yx2@njit.edu, rui.liu@njit.edu, haimin@flare.njit.edu
[2] Max Planck Institut für Sonnensystemforschung (MPS), Max-Planck-Strasse 2, 37191 Katlenburg-Lindau, Germany; wiegelmann@linmpi.mpg.de
Received 2010 May 7; accepted 2010 July 2; published 2010 July 22

ABSTRACT

We present a striking filament pattern in the nonlinear force-free (NLFF) chromospheric magnetic field of the active region NOAA 10956. The NLFF chromospheric field is extrapolated from the *Hinode* high-resolution photospheric vector magnetogram using the weighted optimization method. The modeled structure is characterized by a highly sheared field with strong horizontal magnetic components and has a virtually identical shape and location as the filament seen in Hα. The modeled field strength agrees with the recent He I 10830 Å observations by Kuckein et al.. The unequivocal resemblance between the NLFF extrapolation and the Hα observation not only demonstrates the ability of the NLFF field to reproduce chromospheric features, but also provides a valuable diagnostic tool for the filament magnetic fields.

Key words: magnetic fields – Sun: chromosphere – Sun: filaments, prominences

1. INTRODUCTION

Magnetic diagnostics of solar filaments in the chromosphere are crucial for our understanding of their formation, maintenance, and final eruption. However, due to the intrinsically weak chromospheric magnetic field (Solanki et al. 2006), direct spectropolarimetric measurements of magnetic field vectors in filaments had been extremely rare, difficult, and unreliable for a long time.

The situation has changed with recent advances in near-infrared spectropolarimetric instrumentation. For instance, the Tenerife Infrared Polarimeter (TIP) of the German Vacuum Tower Telescope (VTT, Tenerife, Spain) provides full Stokes spectropolarimetric measurements using the He I multiplet at 10830 Å, which is sensitive to both Hanle and Zeeman effects and opens a new diagnostic window for the study of filament magnetic fields (Casini et al. 2009). In a recent paper by Kuckein et al. (2009), the analysis of TIP He I 10830 Å polarimetry indicates that the magnetic field strengths in an active-region filament range between 600 and 700 G with transverse components of 500–600 G. The result of Kuckein et al. (2009) is one order of magnitude larger than most previous measurements (e.g., Trujillo Bueno et al. 2002; Casini et al. 2003; Merenda et al. 2006). Kuckein et al. (2009) ascribed low values in early measurements to the lack of full Stokes polarimetry and proposed that strong magnetic fields (on the order of magnitude of a few hundred Gauss) might be commonly present in active-region filaments.

On the other hand, sophisticated nonlinear force-free (NLFF) field reconstruction techniques and high-resolution photospheric magnetic field measurements have become available in the last few years; these enable us to extrapolate the chromospheric and coronal magnetic fields from the lower, observable photospheric field. Assuming that the field is free of the Lorentz force (a condition that is generally met without an eruption in progress), the NLFF field is regarded as a fair approximation of chromospheric and coronal magnetic fields (Gary 2001). As a good complement to the He I 10830 Å spectropolarimetric measurements, which are made at one single layer of the solar atmosphere, the NLFF field provides a three-dimensional perspective of magnetic structures in an active region.

In this Letter, we employ an advanced NLFF field modeling method to extrapolate the chromospheric field. We then compare the extrapolation with the simultaneous Hα observation in order to identify vector magnetic fields in the filament. Strong magnetic fields on the order of magnitude of a few hundred Gauss are found in the filament, which is consistent with the recent measurements by Kuckein et al. (2009).

2. Hα OBSERVATION AND NLFF FIELD EXTRAPOLATION

The filament studied in this Letter was located to the south of the active region NOAA 10956. Figure 1(g) shows the Hα image of the active region taken on 2007 May 18 at 05:52 UT by the Solar Optical Telescope (SOT) on board *Hinode*. The target filament is indicated by the arrow.

The Spectro-Polarimeter (SP) instrument of the SOT obtains Stokes profiles of two magnetically sensitive Fe lines at 6301.5 and 6302.5 Å with a sampling of 21.6 mÅ. The *Hinode*/SOT-SP scan of this active region began at 06:06 UT, 2007 May 18 ($\sim$14 minutes later than the Hα observation). The polarization spectra were inverted to the photospheric vector magnetogram using an Unno–Rachkovsky inversion based on the assumption of the Milne–Eddington atmosphere (e.g., Lites & Skumanich 1990; Klimchuk et al. 1992). The vector magnetogram was rebinned to $0\farcs6$ pixel^{-1}.

Before supplying the photospheric vector magnetogram to the extrapolation code, we (1) resolved the 180° azimuthal ambiguity in the transverse field using the "minimum energy" method (Metcalf 1994); (2) removed the projection effects by transforming the vector magnetogram from an observational-plane to a heliographic-Cartesian coordinate. The target was near the solar disk center (2°N, 18°E), so this correction is insignificant; and (3) preprocessed the vector magnetogram (Wiegelmann et al. 2006) so that the photospheric boundary is consistent with the force-free condition. Finally, we applied the "weighted optimization" method (Wiegelmann 2004), one of the best-performing NLFF field modeling methods (Schrijver et al. 2006; Metcalf et al. 2008), to the preprocessed photospheric vector magnetogram to extrapolate the magnetic field toward progressively higher layers.

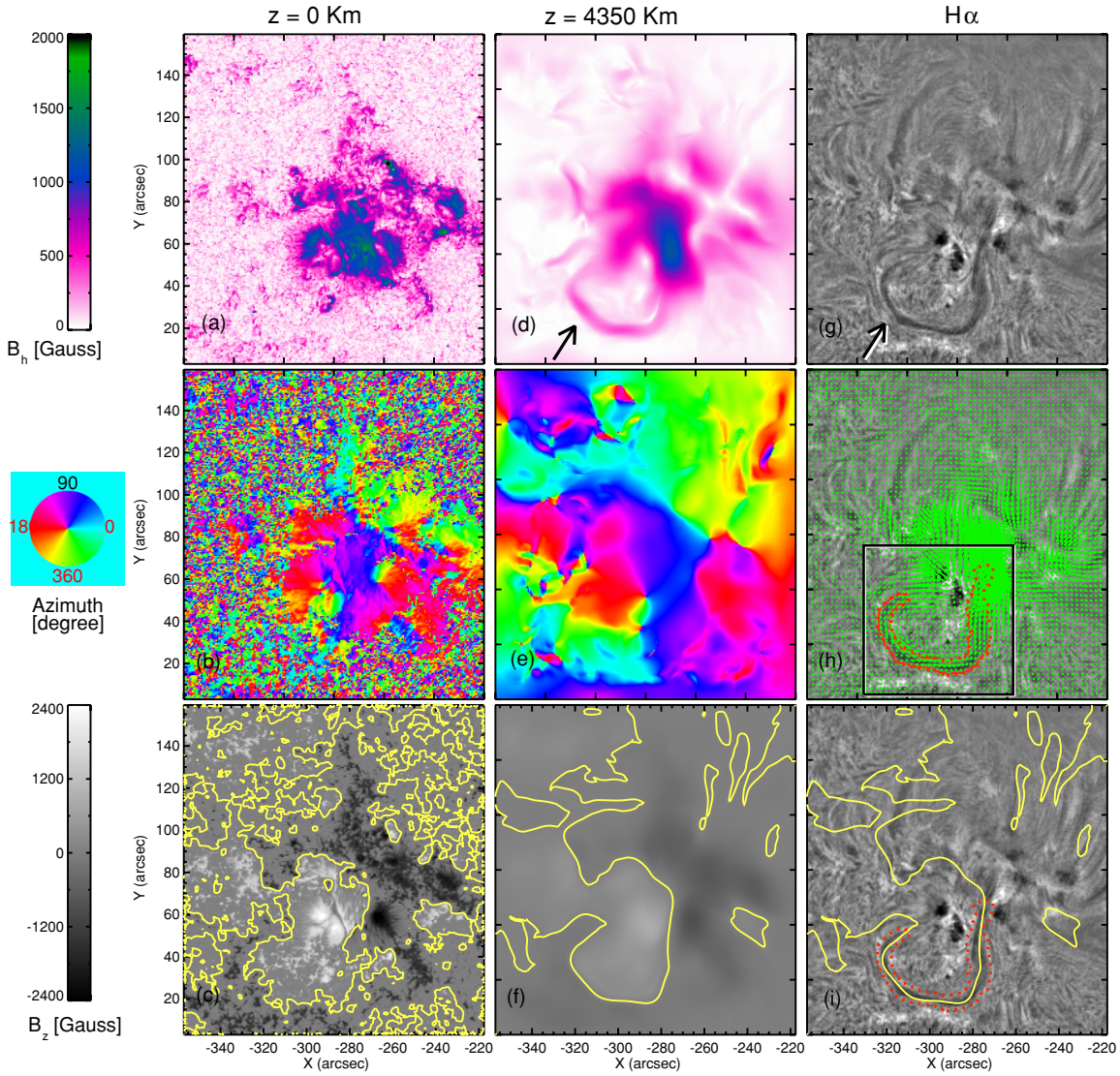

Figure 1. Magnetic fields and Hα observation of the filament of the active region NOAA 10956. Panels ((a)–(c)): the photospheric horizontal field strength, azimuthal angle, and vertical field strength. Panels ((d)–(f)): the chromospheric horizontal field strength, azimuth angle, and vertical field strength at a height of 4350 km. Panels ((g)–(i)): the Hα image of the active region, the same Hα image with overplotted horizontal vectors, and the magnetic PIL at the height of 4350 km. The arrows in panels (d) and (g) indicate the filament structure seen in the extrapolated chromospheric field and Hα observation. The green arrows in panel (h) show the horizontal field vectors. The yellow contours show the magnetic polarity inversion lines (PILs). The red contours mark the location and shape of the filament. The rectangular box in panel (h) is defined for the close-up view displayed in Figures 2 and 3.

The dimensions of the computational domain in this case are $\sim 104 \times 115 \times 44\,\mathrm{Mm}^3$, with a vertical interval of 435 km between layers. The layer at a height of $z = 4350$ km was compared with the Hα observation, as the typical formation height of the Hα line is ~4300–4400 km (Johannesson & Zirin 1996).

3. RESULTS

Figure 1 compares the photospheric/chromospheric magnetic fields (the left/middle columns) with the Hα observation (the right column). A visual inspection immediately reveals a striking filament pattern in the chromosphere ($z = 4350$ km). The pattern (indicated by the arrow in Figure 1(d)) is characterized by strong horizontal magnetic components and has almost the same overall shape and location as the Hα filament. In contrast, the directly observed photosphere ($z = 0$ km) bears no resemblance to the Hα observation. The filament pattern in the chromospheric magnetic field demonstrates (at least in this case) the ability of the NLFF field to successfully reproduce the chromospheric features and allows for further quantitative analysis of the filament magnetic fields.

Figure 2(a) presents a clearer, close-up view of the horizontal field vectors at a height of 4350 km. Evidently, the filament is located along the magnetic polarity inversion line (PIL). The horizontal field vectors within the filament are almost aligned with the magnetic PIL. Here, we define a magnetic shear angle as the angle between the NLFF field and the potential field. Figure 2(b) shows the map of a magnetic shear angle at a height of 4350 km. The filament pattern is highly sheared: the mean shear angle within the filament is 71°.

We further use the extrapolated NLFF field to get the height and field strength information of the filament. The top four panels in Figure 3 show the NLFF horizontal field at different heights. Although the field fades away with an increasing height, the filament pattern can easily be identified at these heights and

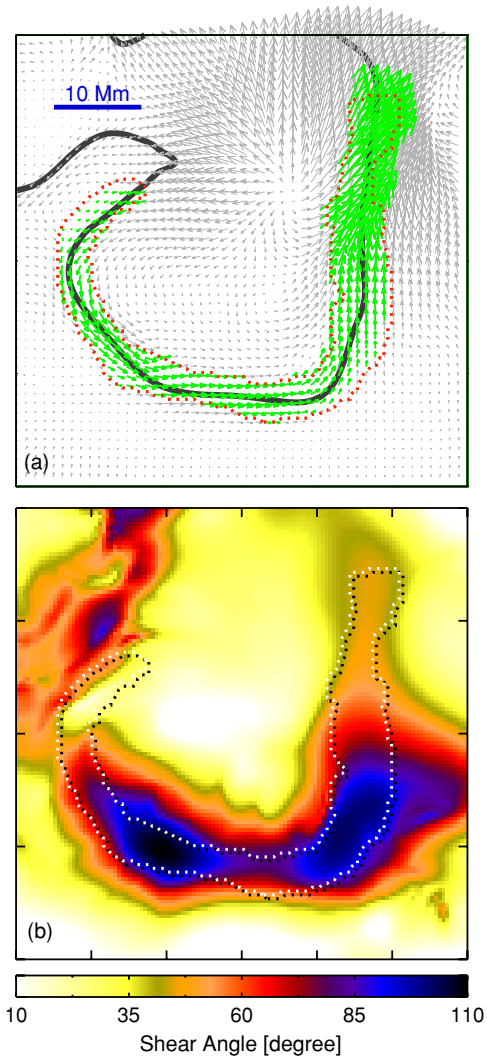

Figure 2. Highly sheared filament magnetic field at a height of 4350 km. Panel (a): a close-up view of the horizontal field vectors (shown as arrows). The length of the arrows is proportional to the strength of the vectors. The direction of the arrows agrees with the direction of the vectors. The black solid and red dotted contours indicate the magnetic PIL and the Hα filament, respectively. The vectors inside the filament contour are highlighted with the green color. Panel (b): the map of a magnetic shear angle. The dotted contour indicates the Hα filament. The FOV of two panels is defined by the box in Figure 1(h).

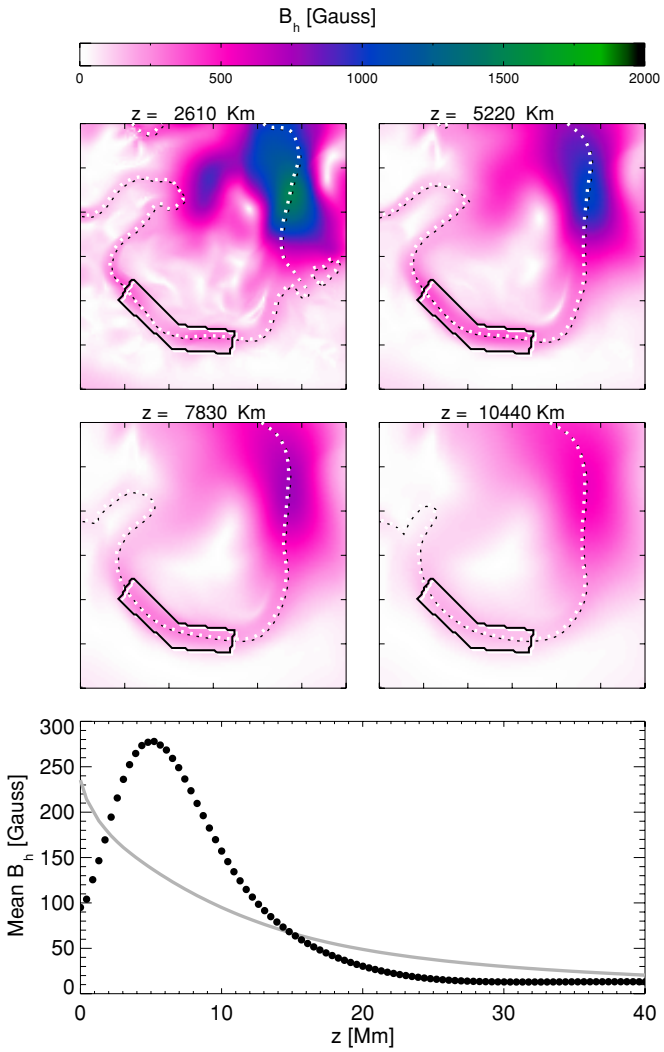

Figure 3. Top four panels: the NLFF horizontal field at different heights, i.e., $z = 2610$, 5220, 7830, and 10,440 km, respectively. The polygon in each panel marks a region of interest (ROI). The FOV of the panels is defined by the box in Figure 1(h). Bottom panel: the mean horizontal field in the ROI (black dots) and the mean horizontal field over the FOV (gray curve) as a function of height.

always resides along the magnetic PIL. The mean horizontal field within the filament pattern (as averaged within the polygons shown in the top four panels) as a function of height is plotted in the bottom panel (the dotted curve). The mean horizontal field over the field of view (FOV) as a function of height is also plotted (the gray curve) as a reference. Despite the continued weakening of the overall horizontal field with height in this active region, the horizontal field in the filament pattern actually increases at first, reaches a maximum at ~5000 km, and then decreases. As a result, we see that the filament pattern first appears vaguely at a height of 2610 km, becomes most noticeable at 3480–6090 km, and then gradually fades away.

In a height range of 3480–6090 km, the magnetic field within the filament structure is of ~200–400 G (with a mean of 320 G), dominated by a horizontal component of ~100–390 G (with a mean of 270 G). Our results are comparable to (although slightly lower than) what Kuckein et al. (2009) measured for an active-region filament, which is of 600–700 G with a horizontal component of 500–600 G. Considering that the filament studied here was located in the periphery of the active region, one should not expect a field as strong as that in Kuckein et al (2009).

With the NLFF field in hand, the electrical current density $|\mathbf{J}|$ ($|\mathbf{J}| = \frac{1}{\mu_0}|\nabla \times \mathbf{B}|$, where μ_0 is the magnetic constant and $\mathbf{B}$ is the vector magnetic field) and the magnetic configuration of the filament are readily deduced. The background image of Figure 4 shows the current density map that was integrated vertically through the computational domain. The filament pattern is also evident on the current density map. We see the presence of a flux-rope configuration in the extrapolated NLFF field. The flux rope, shown as the colored field lines overlaid on the current density map, is generally aligned with the filament and has ~1.5 turns. Such a structure may be critical to understand the eruption of filaments.

4. SUMMARY

To summarize, our application of the NLFF field extrapolation to an active region shows an unequivocal filament pattern in the chromospheric magnetic field. The pattern is virtually identical to the Hα filament in shape and location, and is characterized

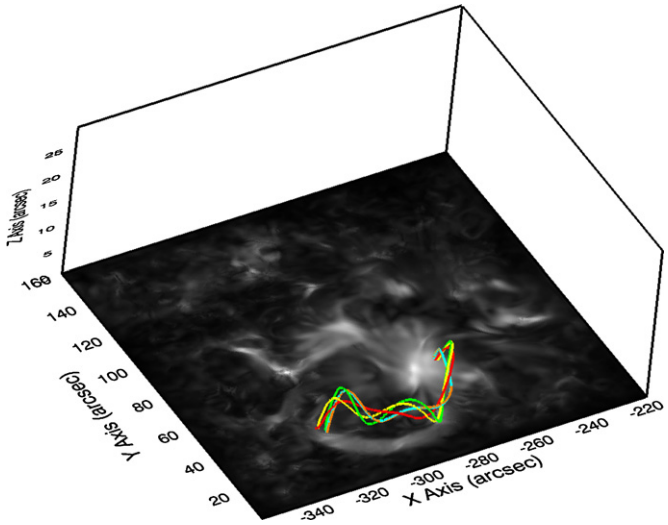

Figure 4. Vertically integrated electrical current density |**J**| map with the overplotted flux rope (colored field lines). The integration of the |**J**| map is throughout the computational domain. The white/black areas in the map show where |**J**| are highest/lowest.

by a highly sheared field with strong horizontal magnetic components.

The particularly good match between observation and extrapolation validates the NLFF field extrapolation and allows for the quantitative analysis of the filament magnetic field. It is found that the filament field can be described as a twisted flux rope. The magnetic field strengths in the filament are ∼200–400 G, significantly larger than most early measurements, but comparable to the recent measurement of Kuckein et al. (2009). Our study provides evidence of the existence of strong magnetic fields (on the order of magnitude of a few hundred Gauss) in active-region filaments.

The authors thank the referee for providing a number of valuable comments that improved this Letter. The authors also thank Yang Guo for helpful discussion. *Hinode* is a Japanese mission developed and launched by ISAS/JAXA, collaborating with NAOJ as a domestic partner, and NASA and STFC (UK) as international partners. J.J., Y.Y., and H.W. were supported by NSF under grants ATM 09-36665, ATM 07-16950, and NASA under grants NNX0-7AH78G and 8AQ90G. Y.X. was supported by NSF under grant ATM 08-39216. T.W. was supported by DLR grant 50 OC 0501.

REFERENCES

Casini, R., López Ariste, A., Tomczyk, S., & Lites, B. W. 2003, ApJ, 598, L67
Casini, R., Manso Sainz, R., & Low, B. C. 2009, ApJ, 701, L43
Gary, G. A. 2001, Sol. Phys., 203, 71
Johannesson, A., & Zirin, H. 1996, ApJ, 471, 510
Klimchuk, J. A., Canfield, R. C., & Rhoads, J. E. 1992, ApJ, 385, 327
Kuckein, C., Centeno, R., Martinez Pillet, V., Casini, R., Manso Sainz, R., & Shimizu, T. 2009, A&A, 501, 1113
Lites, B. W., & Skumanich, A. 1990, ApJ, 348, 747
Merenda, L., Trujillo Bueno, J., Landi Degl'Innocenti, E., & Collados, M. 2006, ApJ, 642, 554
Metcalf, T. R. 1994, Sol. Phys., 155, 235
Metcalf, T. R., et al. 2008, Sol. Phys., 247, 269
Schrijver, C. J., et al. 2006, Sol. Phys., 235, 161
Solanki, S. K., Inhester, B., & Schssler, M. 2006, Rep. Prog. Phys., 69, 563
Trujillo Bueno, J., Landi Degl'Innocenti, E., Collados, M., Merenda, L., & Manso Sainz, R. 2002, Nature, 415, 403
Wiegelmann, T. 2004, Sol. Phys., 219, 87
Wiegelmann, T., Inhester, B., & Sakurai, T. 2006, Sol. Phys., 233, 215